Mechanism for Influence of Nose Bluntness on Asymmetric Vortices

WANG Gang(王刚)*, LIANG Xin-Gang(梁新刚)

Department of Engineering Mechanics, Tsinghua University, Beijing 100084

(Received 7 July 2004)

Pressure distributions on slender bodies are measured at various roll angles; it is found that the side loads on the blunted-nose slender body are as small as one-third of that on a pointed-nose one, or even zero at some roll angles. Numerical simulation shows that different flow structures are generated on the leeside of the bodies with different noses. The results confirm that a structure of U-shaped horseshoe vortex develops on the top of the blunted nose due to the closed type of surface flow separation. The shear layer separated from the nose is entrapped into the horseshoe vortex core and forms two main vortices on the two sides of the body. The function of this structure is to hold in the two main nose vortices and to restrict the emergence of asymmetry.

PACS: 47. 32. Cc, 47. 32. Ff, 47. 85. Gj, 47. 27. Vf

It has been recognized for a long time that asymmetric vortex shedding occurs on slender bodies at high angles of attack, and produces side force and yaw moment on the bodies even at zero side slip.[1,2] Keener *et al.*[3] reported that the local sectional side force can exceed the local sectional normal force by a factor as large as 1.5 on a tangent ogive of fineness ratio 3.5. Such a large force is very harmful to the aircraft such as missile, rocket and modern fighter plane. Therefore some techniques are taken to eliminate or restrain the side loads.[4] Among them, the nose geometry and its bluntness are found to exert an important influence on the asymmetric vortices' flow field and their induced asymmetric loads.[1,5] Thus, some researchers have devoted great effort to the nose geometry. Cones with cross section of circular, elliptic, biparabolic and biwedge were introduced by Siclari to study the flow field of different forebodies.[6] A dozen noses with different geometries and bluntness were adopted by Brandon and Nguyen to research the stability of a fighter model with a cylindrical fuselage shape.[7]

There are two kinds of nose geometries, one is of axis-asymmetric cross section, and the other is axisymmetric cross section. For the former kind, the sharp edges along the nose cause the separation points to be fixed like a straked nose, or the asymmetric boundary alters the flow condition like an elliptic sectional nose. The flow structures of these types are different from the original ones. For the latter kind, the nose bluntness was found to make the side loads significantly decrease. On a slender body with a pointed nose, the vortex asymmetry usually begins from the nose, and the vortices shed at a relatively rapid rate causing alternating side force distribution along the long body. The inception angle of asymmetry α_{AV} is relatively lower. On the slender body with a blunted nose, the vortex asymmetry and its side force usually begins from the afterbody, and then move to the nose with the angle of attack increasing. The angle α_{AV} is relatively higher. Ericsson and Reding[1] believed that a slight amount of nose bluntness variance, as little as 6%, can cause the transformation of types of vortex shedding. Pick indicated that nose bluntness is an effective means of reducing the side force,[8] but the physical mechanism has not been completely understood. Many researchers only ascribed the cases in the absence of a sharp nose tip.

How are the flow field and its side loads affected by the nose bluntness? In the tests by Yanta and Wardlaw,[9] a sharp nose tip was replaced with a 10% spherically blunt one, and their results showed that it did significantly reduce side forces but the nose bluntness was not found to fundamentally change the leeward flow fields. The flow field of a blunted model is more stable than that of a sharp model and the resulting degree of asymmetry is too small to produce vortex shedding. The reason for this remains unclear. However, Hunt *et al.* observed that the nose, whether pointed or blunted, may not be the basic geometric characteristic to differentiate the separation type, while the curvature of nose contour might be the important factor.[10]

By surface pressure measurement, oil flow test and numerical simulation of flow field, a systematic study of the flow structure of two models are performed. Different side force distributions for bodies with different noses are reported and the mechanism for the influence of nose bluntness on the asymmetric vortix structure is presented in this Letter.

The test models designed are two cylindrical afterbodies with two interchangeable noses, the pointed and blunted noses, both of which are tangent ogives and made of the same counter except that the blunted one has a bluntness of 20% at the top end, so the fineness ratio of pointed nose is $L_N/D = 3.0$ and that

* Email: wangangwwy@mail.tsinghua.edu.cn

©2004 Chinese Physical Society and IOP Publishing Ltd

of blunted nose is $L_N/D = 2.776$. Two afterbodies are of the same length with $L_A/D = 9.14$. One is for pressure measurement with 18 taping stations, and the other is for oil flow test. Experiments are conducted by streaking in the wind tunnel of Peking University and by pressure measurement in wind tunnel NF-3 of Northwest Polytechnic University. For more information of the models and test facilities, please consult Ref. [11]. The working Reynolds number is $R_e = V_\infty \cdot D/\nu = 1.0 \times 10^5$, which keeps the flow around the slender bodies in the range of subcritical Reynolds.[12] The variation of the angle of attack is from 0° to 70°. The same physical models are used in our numerical simulations. The calculations are performed by solving the continuum Navier–Stokes equations for incompressible laminar flow with a finite volume method incorporating the third-order-accurate discretization scheme CFL3D. This numerical code was originally developed by Thomas *et al.*[13] The conservation form of the governing equations in generalized coordinates (ξ, η, ζ) can be written as

$$\frac{\partial}{\partial t}(Q)+\frac{\partial}{\partial \xi}(F-F_v)+\frac{\partial}{\partial \eta}(G-G_v)+\frac{\partial}{\partial \zeta}(H-H_v)=0,$$

where $Q = (J^{-1})\ (\rho, \rho u, \rho v, \rho w, e)^T$; F, G and H are the inviscid flux vectors, F_v, G_v, H_v represent the viscous terms, and J is the Jacobian expression $\partial(\xi, \eta, \zeta)/\partial(x, y, z)$.[13]

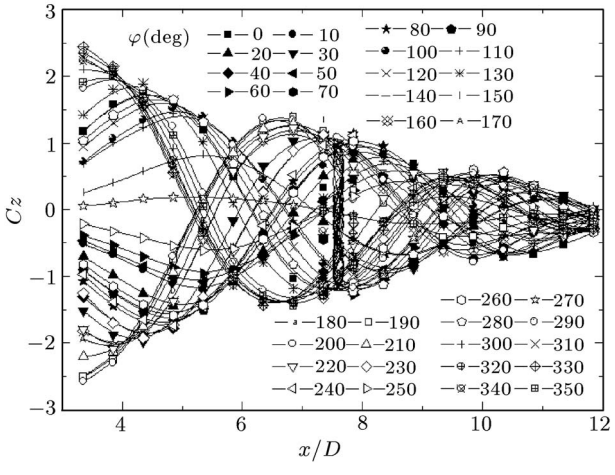


Fig. 1. Side force distribution on pointed-nose slender body.

At lower incidence ($\alpha = 10°$), the side force coefficient is zero since the generated vortex pair is symmetric at leeward of the pointed-nose and blunted-nose slender bodies. Our oil flow results indicate that both the surface separation types are of the open ones on the two models. The side force distributions on the pointed-nose slender body at the high incidence ($\alpha = 50°$) and different roll angles are presented in Fig. 1. It shows that all the curves are quasi-sinusoid with swings decaying to nearly zero after three or four half-cycles. The variation of the curve phases with roll angles suggests that the inception angles of asymmetry are different. The magnitude of side force coefficients is normally within the range of $1 < |C_z| < 3.5$. The side force distributions on the blunted-nose model for the same conditions are shown in Fig. 2. It can be seen that their characteristics differ greatly from those in Fig. 1 though the curves are still sinusoidlike. The phases of different curves are basically the same in Fig. 2, so are the axial positions of zero points.

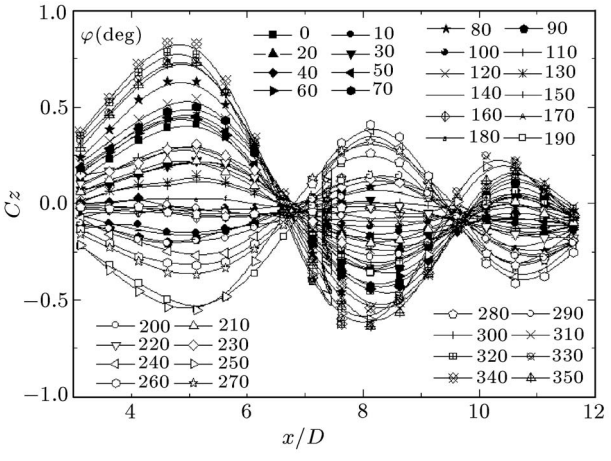


Fig. 2. Side force distribution on blunted-nose slender body.

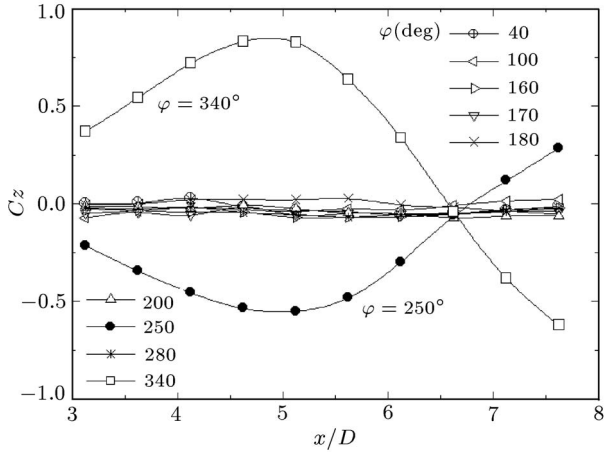


Fig. 3. Zero value of C_z on blunted-nose slender body.

It should be noticed that the magnitude of side force coefficients for the blunted nose is within the range of $|C_Z < |1$, which is significantly lower than that generated on the pointed nose model. The more curious and fascinating phenomenon is that a series of nearly zero side force coefficients occurs with the variation of roll angle as shown in Fig. 3, where roll angle $\varphi = 40°, 100°, 160°, 170°, 180°, 200°, 280°$. For comparison, two curves $(\varphi = 250°, 340°)$ that have a large C_z are also given in Fig. 3. Now the test inter-

val of roll angle is 5°, and we can foresee that more states of zero value of C_z will be produced by reducing the test interval of roll angles. What causes such different characteristics of side loads on two different noses with the same cylinder afterbody? Is the flow field developed on the blunted nose model completely different from that on the pointed nose one?

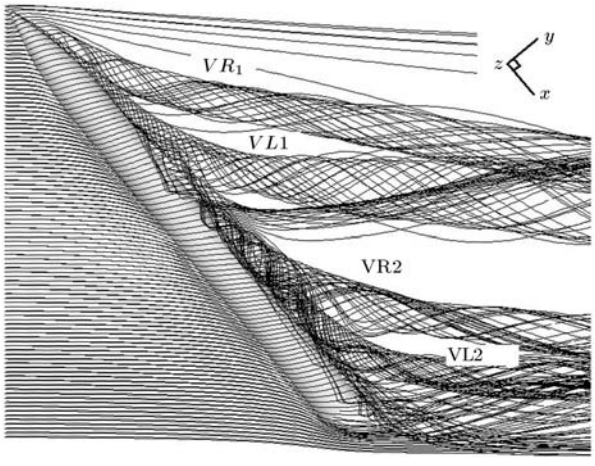


Fig. 4. Vortices' system over pointed-nose slender body ($\alpha = 50°$).

Our numerical results indicate that on the pointed nose model, the main vortex pair originated from the nose boundary layer separation becomes asymmetric at high incidence ($\alpha = 50°$), with one vortex in a higher position and its counterpart in a lower position. Developing downstream along the body, the higher vortex will eventually shed from the model and be replaced by a new vortex originating from the body boundary layer separation. Such a process continues right-and-left alternately, finally an asymmetric multivortex system is established as shown in Fig. 4, which produces a quasi-sinusoidal distribution of side force (Fig. 1). The pertinence between the vortices system and its induced side loads has been studied experimentally by Deng *et al.*[14]

The results also show that on the blunted nose model, the two vortices keep a symmetric state basically downstream along the body at some roll angles ($\varphi_{C_z=0}$) and high incidence ($\alpha = 50°$), which produces nearly zero value of C_z as shown in Fig. 3. However, they also become asymmetric at other roll angles ($\varphi_{C_z\neq 0}$) and then develop into a vortex series which is similar to that on the pointed-nose model. The interval of the vortex series on the blunted-nose model is smaller than that on the pointed-nose model, which results in smaller values of C_z as shown in Fig. 2.

What causes such different flow structures on the two models? Could a slight discrepancy only on the tip of the noses produce a fundamental transition of the flow behaviour?

In order to understand the nature of the flow field, surface flow patterns are investigated firstly over the two slender bodies. Figures 5 and 6 show the tested oil flow patterns on the two different noses. It can be seen that both the primary and secondary separation lines are of the open type on the pointed nose (Fig. 5), whereas they are of the closed type on the blunted nose (Fig. 6). Such different types of separation have been known extensively. However, how do they influence the development of spatial structure over the whole models?

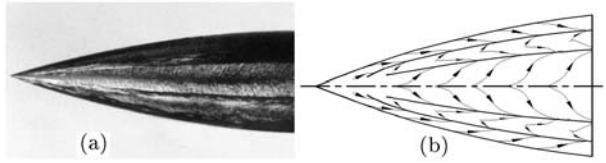


Fig. 5. Oil flow pattern on pointed nose.

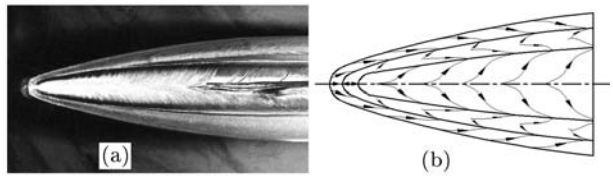


Fig. 6. Oil flow pattern on blunted nose.

The numerical simulation indicates that a structure of U-shaped horseshoe vortex forms on the leeside of the blunted nose due to the closed separation (Fig. 7). This vortex structure was also observed in our tests of flow visualization in the water tunnel of Beijing University of Aeronautics and Astronautics. Here we present the computational results, from which one can clearly perceive its configuration. A U-shaped horseshoe vortex, which only originates from closed separation of a blunted nose top, entraps the separated shear layer rolling up from the two sides of the nose into its core directly, and forms two main vortices (VR1 and VL1) on the two sides of the body rotating in opposite directions. Thus the two main vortices have a common joint end at the top of the nose. The structure of the U-shaped horseshoe vortex provides a relatively settled vortex core for the two main vortices as shown in Fig. 8. For a pointed nose, since no such vortex structure forms due to the open separation, the trajectories of the two main vortices are independent of each other as shown in Fig. 9.

The flow field around a slender body is very sensitive to the disturbance from the minute irregularities on or near the nose tip which are produced from the model machining tolerance,[11] and such disturbance is usually uneven and inevitable. Without the restriction of the U-shaped horseshoe vortex, the two main vortices VR1 and VL1 can easily become asymmetric at the nose disturbance with a larger vortex interval

and develop into an asymmetric multi-vortex series as shown in Fig. 4, causing higher side loads on the pointed-nose slender body (Fig. 1).

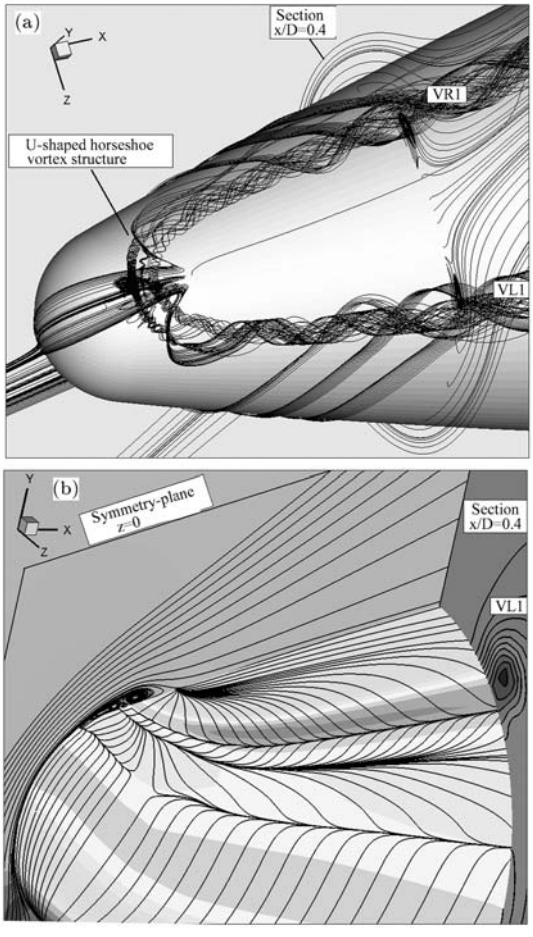


Fig. 7. A structure of U-shaped horseshoe vortex formed at the leeside of blunted nose top.

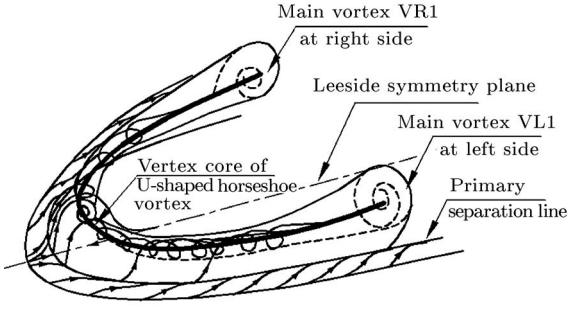


Fig. 8. Sketch of vortex structure at the leeside of blunted nose.

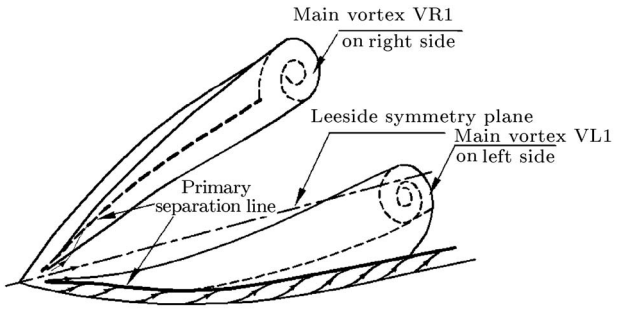


Fig. 9. Sketch of vortex structure at the leeside of pointed nose.

For the blunted-nose slender body, even if the disturbance also exists in the nose top, the two main vortices VR1 and VL1 are inclined to remain symmetric with the restriction of their U-shaped horseshoe vortex structure locating at the nose top. Therefore at some roll angles where side loads are nearly zero ($\varphi_{C_z=0}$), the state of VR1 and VL1 is basically symmetric downstream along the slender body. However, the state of the two main vortices is just held in or restricted, not locked in by their U-shaped horseshoe vortex. Thus, at other roll angles at which the side loads are not zero ($\varphi_{C_z\neq 0}$), the two main vortices also become asymmetric and a series of vortices similar to Fig. 4 are generated with a relatively small vortex interval, which produces small side loads as shown in Fig. 2. The difference of the effects of the U-shaped horseshoe vortex between the two states, $\varphi_{C_z\neq 0}$ and $\varphi_{C_z=0}$, will be further studied in the future.

References

[1] Ericsson L E and Reding J P 1985 *AIAA*-85-1797
[2] Luo S C, Lim T T, Lua K B, Chin H T, Goh E K R and Ho Q W 1998 *AIAA J.* **36** 1778
[3] Keener E R, Chapman G T, Cohen L and Talaghani J 1977 NASA TMX-3437
[4] Williams D 1997 *AIAA*-97-1967
[5] Pick G S 1971 *AIAA*-71-570
[6] Siclari M J 1992 *AIAA J.* **30** 124
[7] Brandon J M and Nguyen L T 1986 *AIAA*-86-0331
[8] Pick G S 1971 *AIAA*-71-570
[9] Yanta W J and Wardlaw A B 1982 *AIAA*-82-0343
[10] Hunt B L, Northrop Corp and Hawthorne CA 1982 *AIAA*-82-1336
[11] Wang G, Deng X Y, Liu P Q and Wang Y K 2004 *Acta Aerodynam. Sin.* **22** 7 (in Chinese)
[12] Lamont P J and Hunt B L 1976 *J. Fluid. Mech.* **76** 519
[13] Thomas J L, Krish S T and Anderson W K 1990 *AIAA J.* **28** 205
[14] Deng X Y, Wang G, Chen X R et al 2003 *Sci. Chin.* E **46** 561